scientific reports

Check for updates

OPEN

A lncRNA and radiomics-based model for predicting the response of non-small cell lung cancer to chemo- and radio-therapy

Fang Ye[1,2], Yi Yin[2], Jiexiao Wang[2,3], Jialiang Wang[2,3], Jie Yang[2], Jun Zhang[4], Yani Zhang[1,2], Jian Qi[1,2], Qizhi Zhu[1], Yucheng Zhang[2], Haifen Ji[2], Zongtao Hu[2], Bo Hong[1,2,3]✉ & Hongzhi Wang[1,2,3]✉

This study aimed to identify a novel plasma lncRNA biomarker and establish a model based on lncRNAs and radiomics for predicting the response of non-small cell lung cancer (NSCLC) to chemo- and radio-therapy. Next-generation sequencing and integrated bioinformatics analysis were used to identify lncRNAs associated with the response of NSCLC to chemo- and radio-therapy. RT-qPCR was utilized to detect MIF-AS1 expression in the plasma of NSCLC patients. Radiomics analysis was performed on CT images of NSCLC patients. The model was constructed by multiple logistic regression. The expression of the lncRNA MIF-AS1 was up-regulated in the plasma of patients with chemo- and radio-resistant NSCLC, as validated by RT-qPCR in 124 NSCLC patients. Furthermore, in vitro experiments demonstrated that knockdown of MIF-AS1 expression significantly reduced cellular proliferation and invasion, and increased the sensitivity of NSCLC cells to the chemotherapeutic drug cisplatin. Using the ceRNA network, a DNA-damage repair related protein RAD21 was identified as a target gene of MIF-AS1. Finally, two radiomic features were found to be associated with the response of NSCLC to chemo- and radio-therapy. Combining the MIF-AS1 level and the two radiomic features, a model was established to predict the response of NSCLC to chemo- and radio-therapy, with a high AUC of 0.808. MIF-AS1 could be a novel biomarker for predicting the response of NSCLC to chemo- and radio-therapy. This model, which uses both CT radiomics and MIF-AS1 levels, increases the accuracy of predicting therapeutic response in NSCLC patients.

Keywords LncRNA, MIF-AS1, Non-small cell lung cancer, Non-invasive diagnosis, Biomarkers

Lung cancer is the most common malignancy and the leading cause of cancer-related mortality globally, posing a grave threat to human health. Non-small cell lung cancer (NSCLC) is the predominant subtype of lung cancer, accounting for approximately 85% of all cases. However, despite considerable therapeutic advances, the prognosis for NSCLC patients remains poor, with a five-year survival rate of only about 15%[1]. The lack of symptoms in early-stage NSCLC is a key factor contributing to its poor prognosis. As a result, a majority of patients are not diagnosed until the disease has reached an advanced stage with distant or lymphatic metastasis[2]. For NSCLC patients lacking actionable mutations, the first-line treatment typically consists of platinum-based chemotherapy with radiotherapy[3]. Yet, no reliable biomarkers are available to predict patient response to these therapies, which remains an unmet clinical need.

Long non-coding RNAs (LncRNAs), a class of non-coding transcripts exceeding 200 nucleotides in length, play crucial roles in various human diseases, including cancer. Furthermore, their aberrant expression has been closely linked to the development, invasion, and metastasis of NSCLC[4,5]. Liu et al. demonstrated that the expression of the long non-coding RNA MNX1-AS1 was up-regulated in NSCLC, and its elevated expression was significantly associated with advanced tumor stage, lymph node metastasis, and poor prognosis in NSCLC patients. Moreover, knockdown of MNX1-AS1 markedly suppressed the proliferation, migration, and invasion of NSCLC cells[6]. Accumulating evidences have indicated that a variety of lncRNAs are involved in tumor chemo-

[1]University of Science and Technology of China, Hefei, Anhui, China. [2]Hefei Cancer Hospital of CAS, Institute of Health and Medical Technology, Hefei Institutes of Physical Science, Chinese Academy of Sciences (CAS), Hefei, Anhui, China. [3]School of Basic Medical Sciences, Anhui Medical University, Hefei, Anhui, China. [4]Hefei Innovation Research Institute of Beihang University, Hefei, Anhui, China. ✉email: bhong@hmfl.ac.cn; wanghz@hfcas.ac.cn

and radio-resistance by mediating DNA damage repair, apoptosis, and tumor stem cell activity[7,8]. For example, lncRNA-XIST conferred resistance to cisplatin in NSCLC cells via dual pathways involving miR-17/autophagy and let-7i/BAG-1, ultimately suppressing apoptosis and promoting proliferation[9]. The lncRNA-CRNDE, in complex with PRC2, conferred radiotherapy resistance in lung adenocarcinoma by regulating p21 expression[10]. Moreover, Liu et al. reported that the lncRNA ANRIL contributed to chemoradiotherapy resistance in NSCLC by mediating enhanced DNA repair through homologous recombination[11]. Thus, lncRNAs play key roles in regulating the proliferation, metastasis, and treatment resistance of tumor cells.

Furthermore, recent studies have demonstrated that tumor-derived exosomal lncRNAs are consistently present in human blood. Since they can be detected non-invasively and readily in blood, lncRNAs consequently hold great promise as biomarkers for early cancer detection, monitoring disease progression, and assessing prognosis[12,13]. Previous studies have shown that a combination of serum lncRNA biomarkers (SOX2OT and ANRIL) and tumor markers (SCC, CYFRA21-1 and CEA) had high specificity (79.2%) and sensitivity (77.1%) for NSCLC diagnosis[14]. Lin et al. demonstrated that the plasma exosomal lncRNA UEGC1, which originates from gastric cancer cells, was a highly sensitive biomarker for detecting early-stage gastric cancer[15]. Ling et al. reported that the serum lncRNA RP5-977B1 in NSCLC patients exhibited excellent diagnostic value for early detection with an area under the ROC curve (AUC) of 0.890, and that its expression level was further correlated with poor prognosis ($p = 0.036$)[16]. Therefore, blood exosomal lncRNAs hold promise as biomarkers for predicting the response of NSCLC to chemo- and radio-therapy.

Advances in bioinformatics and artificial intelligence have enabled the use of radiomics for predicting responses to cancer therapy[17]. Radiomics involves the high-throughput extraction of quantitative features (including morphology, density, intensity, and texture) from clinical computed tomography (CT) scans. Studies suggest a potential correlation between these deep imaging features and therapeutic outcomes[18]. Subsequently, machine learning algorithms can model these features to accurately predict individual patient responses to cancer therapy[19].

In this study, using plasma exosomal lncRNA sequencing and bioinformatics analysis, we identified lncRNAs potentially mediating chemo- and radio-resistance in NSCLC. We identified and validated the lncRNA MIF-AS1 as a biomarker to predict the therapeutic response in NSCLC. Furthermore, CT image-based radiomic features were integrated with MIF-AS1 to construct a more precise predictive model. This integrated approach increases the accuracy of predicting tumor sensitivity to chemo-and radio-therapy in NSCLC.

Methods

Patients and samples collection

This study included 130 NSCLC patients hospitalized at the Thoracic Cancer Center at Hefei Cancer Hospital, Chinese Academy of Sciences, between 2021 and 2023. Patients were enrolled based on the following criteria: 1) first diagnosis of lung adenocarcinoma or lung squamous cell carcinoma; 2) inoperable stage I-Ⅳ NSCLC; 3) planned treatment involving chemotherapy or radiotherapy. Patients planned to receive targeted therapy or immunotherapy were excluded. Before the chemo- and radio- treatment, 10 mL of blood was drawn. The plasma samples were separated within 6 h and then frozen at -80 °C. This study was approved by The Ethics Committee of Hefei Cancer Hospital of the Chinese Academy of Sciences (Approval number: SL-PJ2023-098). All ethical regulations relevant to human research participants were followed. Before plasma samples were collected, all patients signed a written consent form. This study was performed in compliance with the Declaration of Helsinki.

Next-generation sequencing of exosomal lncRNAs

Plasma exosomal RNA was extracted using an Exosome Isolation Kit (Ribo, Guangzhou, China). According to the manufacturer's instructions of the NEB Next Ultra RNA Library Prep Kit for Illumina (Illumina, CA, USA), RNA was fragmented and converted into first- and second-strand cDNA, followed by amplification and enrichment through ligation and low-cycle PCR. The quality of the libraries was assessed using an Agilent 2200 TapeStation (Agilent, USA) and a Qubit fluorometer (Thermo Fisher, USA). Finally, the libraries were sequenced using an Illumina Nova sequencer (Illumina, CA, USA) with a double-ended 150 bp read length. After the raw sequencing data were obtained, the reads were trimmed using Trim Galore (v0.6.7). The reference genome and annotation GTF file of Homo sapiens Ensembl Version GRCh37.75 were downloaded from the ENSEMBL FTP site (https://ftp.ensembl.org/pub/release-75/). The clean reads were aligned to the GRCh37.75 genome using STAR (v2.7.10b) and then quantified using RSEM (v1.3.1). The edgeR software suite was used to standardize and analyze the differentially expressed lncRNAs between the two groups. The criteria for differentially expressed lncRNAs was $|\log FC| > 0.5$ and $FDR < 0.01$.

Differential expression analysis of lncRNAs between cisplatin-sensitive and resistant NSCLC cell lines

RNA expression data of NSCLC cell lines were obtained from the Genomics of Drug Sensitivity in Cancer (GDSC, version 8.3) database. Based on cisplatin IC50 values, the NSCLC cell lines were classified into two groups: cisplatin-sensitive ($IC50 < 20$; $n = 12$) and cisplatin-resistant ($IC50 > 20$; $n = 37$). LncRNAs were annotated using seqmap software. Differentially expressed lncRNAs between cisplatin-sensitive and cisplatin-resistant NSCLC cell lines were analyzed, according to $p < 0.05$ (Wilcoxon test).

Quantification of lncRNAs using RT-qPCR

The RNA extraction kit (TIANGEN, Beijing, China) was used to extract total RNA from patients' plasma. The total RNA was reverse-transcribed into cDNA using the mRNA/lncRNA qRT-PCR Starter kit (Ruibo, Guangzhou, China). The cDNA was amplified using an ABI7500 fluorescence quantitative PCR instrument (ABI, CT, USA), with 40 cycles of pre-denaturation at 95 °C for 10 min, denaturation at 95 °C for 5 s, annealing

at 60 °C for 30 s, and extension at 72 °C for 30 s. λpolyA + RNA-A was used as an internal standard, and the data were analyzed using the $2^{-\Delta\Delta CT}$ method. All the primers used are listed below:

MIF-AS1 Forward Primer: 5'-CGACCTCGCTCCCCAATATC-3'.

MIF-AS1 Reverse Primer: 5'-AGAGACTAGGAGTGCCTCGG-3'.

Transfection of siRNA

NSCLC cells were seeded in 6-well plates and allowed to adhere for 24 h. Subsequently, the cells were transfected with either MIF-AS1 siRNA or control siRNA (both from GIMMA, Shanghai, China) for 48 h using Lipofectamine 2000 Transfection Reagent (Thermo Fisher, MA, USA). MIF-AS1 knockdown was verified by quantitative RT-qPCR. All the MIF-AS1 siRNA sequences used are listed below:

MIF-AS1-1: 5'-GACGAUACUUCUCAUUUGUTT-3'

5'-ACAAAUGAGAAGUAUCGUCTT-3'

MIF-AS1-2: 5'-GGCACUCCUAGUCUCUAAATT-3'

5'-UUUAGAGACUAGGAGUGCCTT-3'

Cell viability assay

NSCLC cells were seeded in 96-well plates at 1,000 cells per well and cultured for 5 days. Cell viability was assessed daily from day 0 to day 5 using the CellTiter-Glo Luminescent Assay (Promega, WI, USA), with luminescence readings normalized against the values obtained on day 0.

Apoptosis assay

After treatment with cisplatin (10 μg/mL) or vehicle control, apoptosis in NSCLC cells was assessed using a FITC Annexin V Apoptosis Detection Kit (BD Pharmingen, CA, USA). Apoptotic cells were detected by flow cytometry (Beckman Coulter, CA, USA), and data were analyzed with CytExpert software (Beckman Coulter, CA, USA).

Cell scratch experiment

Following a 24-h transfection with MIF-AS1 or control siRNA, a straight wound was introduced in the NSCLC cell monolayer using a pipette tip. After washing twice with PBS to remove dislodged cells, wound closure was monitored at 0, 3, 6, 12, and 24 h under a microscope (Leica Microsystems, Germany). The migration distance was quantified automatically using the MShot Image Analysis System software (Guangzhou, China).

Cell invasion assay

Cell invasion was assessed using Matrigel-coated Transwell chambers (Corning, NY, USA). NSCLC cells in serum-free RPMI 1640 were plated in the upper chamber and incubated for 24 h with RPMI 1640 containing FBS in the lower chamber. The invaded cells on the lower surface were then fixed with paraformaldehyde, stained with 0.1% crystal violet, and visualized under a microscope (Leica Microsystems, Germany).

Western blot

Total protein was extracted from PC9 NSCLC cells with a lysis buffer supplemented with 1 × protease inhibitor (Beyotime, Shanghai, China). Protein samples (20 μg per lane) were separated by 10% SDS-PAGE and transferred onto PVDF membranes. The membranes were blocked with 5% non-fat milk in TBST for 2 h at room temperature and then incubated overnight at 4 °C with the following primary antibodies: anti-Rad21 rabbit monoclonal antibody (Absin, Shanghai, China; 1:1000) and anti-β-Actin mouse monoclonal antibody (Proteintech, Wuhan, China; 1:5000). After washing three times with TBST, the membranes were probed with horseradish peroxidase-conjugated goat anti-rabbit/mouse secondary antibody (Cell Signaling Technology, USA; 1:3000) for 1 h at room temperature. Protein bands were visualized using an ECL detection kit (Beyotime, Shanghai, China).

CT radiomics analysis

Chest CT images for 38 NSCLC patients from TCGA were retrieved from The Cancer Imaging Archive (TCIA). Chest CT images of 124 NSCLC patients were retrospectively collected from the Picture Archiving and Communication System (PACS; CAREstream Medical Ltd.) at Hefei Cancer Hospital, Chinese Academy of Sciences. The inclusion criteria were as follows: 1) a confirmed pathological diagnosis of NSCLC, and 2) availability of pretreatment chest CT scans with good image quality.

CT images were imported into AccuContour software (version 3.1; Manteia, Fujian, China) for feature extraction, with a longitudinal window setting of width 400 and level 40. Tumor regions were manually delineated on each slice by a pulmonologist and a thoracic surgeon, with subsequent review of all regions of interest (ROI) by a radiologist. Subsequently, all radiomic features were standardized using z-scores to minimize dimensional differences, thereby improving model accuracy and centering the feature values around zero. For each NSCLC patient, 1409 radiomic features were extracted.

Feature selection was performed using Least Absolute Shrinkage and Selection Operator (LASSO) regression to identify radiomic features associated with radio- and chemo-therapy response. Subsequently, a predictive model was developed via multivariate logistic regression and graphically presented as a nomogram.

Bioinformatics and statistical analysis

The bioinformatics analyses in this study were performed in the R programming environment (version 4.0.2), utilizing relevant software packages for each specific task. The competing endogenous RNA (ceRNA) network was constructed with the igraph and ggraph packages. Functional enrichment of the network was assessed through Gene Ontology (GO) and Kyoto Encyclopedia of Genes and Genomes (KEGG) pathway analyses.

Kaplan–Meier (KM) curve was used to compare survival differences between the two groups. The predictive accuracy of the model was evaluated using the receiver operating characteristic (ROC) curve, with the optimal cutoff value determined by Youden's index. To assess the clinical application of the predictive model, we employed decision curve analysis (DCA) to evaluate its net benefit. Using nonparametric Mann–Whitney U test, the relative expression level of lncRNA MIF-AS1 in the plasma of NSCLC patients was compared between two groups. For other comparisons, differences between two groups were assessed using the Student's t test for parametric data and the Wilcoxon test for non-parametric data. Comparisons across multiple groups were conducted using one-way analysis of variance (ANOVA), followed by Dunnett's post hoc test. A p-value of less than 0.05 was considered statistically significant.

Results

Identification of the lncRNA MIF-AS1, whose expression is up-regulated in the plasma of chemo- and radio-resistant NSCLC patients

In this study, plasma samples were collected from 6 NSCLC patients, 3 of whom were sensitive to chemo- and radio-therapy, and 3 of whom were resistant to chemo- and radio-therapy (Table S1). The exosome RNAs were isolated and sequenced for lncRNA using a next-generation sequencing (NGS) approach. Differentially expressed lncRNAs were analyzed with the criteria of $|\log FC| > 0.5$ and $FDR < 0.01$. Finally, 5189 differentially expressed lncRNAs were identified (Table S2). To identify the lncRNAs associated with chemo- and radio-resistance, we further screened lncRNAs that were associated with the survival of NSCLC patients in the TCGA database. A total of 430 lncRNAs were found to be significantly associated with the survival of NSCLC patients. Finally, we screened lncRNAs that were differentially expressed between NSCLC normal and tumor tissues in the TCGA database. A total of 203 lncRNAs were found to be significantly up- or down-regulated in NSCLC tumors (Fig. 1A). The expression heatmap of the 203 lncRNAs in the 6 NSCLC patients was shown in Fig. 1B.

Moreover, we collected the IC50 values and gene expression data of NSCLC cell lines from the GDSC database. The 49 NSCLC cell lines were divided into 12 cisplatin-sensitive and 37 cisplatin-resistant cell lines. We examined the differences in lncRNA expression between the sensitive and resistant groups. 15 lncRNAs were differentially expressed, with the p values < 0.05 (Fig. 1A). The expression heatmap of the 15 lncRNAs in the 49 NSCLC cell lines was shown in Fig. 1C.

The 203 lncRNAs identified in NSCLC clinical samples and the 15 lncRNAs identified in NSCLC cell lines were intersected, resulting in the identification of the lncRNA MIF-AS1 (Fig. 1A). In the TCGA database, higher expression of MIF-AS1 was significantly associated with poorer overall survival and progression-free survival of NSCLC patients (Fig. 1D). The expression of MIF-AS1 was up-regulated in NSCLC tumors, compared with normal tissues (Fig. 1E). In the GDSC database, the expression of MIF-AS1 was also elevated in cisplatin-resistant NSCLC cell lines, compared with cisplatin-sensitive NSCLC cell lines (Fig. 1F). In summary, the lncRNA MIF-AS1 is identified to be a potential biomarker for predicting the sensitivity to chemo- and radio-therapy in NSCLC.

Knockdown of MIF-AS1 inhibits cellular proliferation and invasion, as well as increases cisplatin-induced apoptosis in NSCLC

To investigate the oncogenic function of MIF-AS1 in NSCLC, we knocked down MIF-AS1 by siRNA transfection in NSCLC cells. After PC9 and H1299 NSCLC cells were transfected with MIF-AS1 siRNA, RT-qPCR analysis indicated that the expression level of MIF-AS1 was down-regulated (Fig. 2A). Cell viability assay indicated that the ability of cell proliferation was reduced in PC9 and H1299 cells transfected with MIF-AS1 siRNA, compared with cells transfected with control siRNA (Fig. 2B). Next, Matrigel invasion and cell scratch assays were performed to assess the effects of MIF-AS1 on invasion and cell motility. Matrigel invasion assay indicated that knockdown of MIF-AS1 inhibited the invasion of PC9 and H1299 NSCLC cells (Fig. 2C). Cell scratch assay indicated that knockdown of MIF-AS1 inhibited the motility of PC9 and H1299 NSCLC cells (Fig. 2D). We further investigated the effect of MIF-AS1 on cisplatin-induced apoptosis in NSCLC. Annexin V apoptosis assay indicated that the cellular apoptosis induced by cisplatin was significantly increased when PC9 and H1299 cells were transfected with MIF-AS1 siRNA, compared with cells transfected with control siRNA (Fig. 3). Therefore, these results indicate that MIF-AS1 downregulation suppresses the proliferative and invasive capacities of NSCLC cells and sensitizes them to cisplatin-induced apoptosis.

The identification of RAD21 as a target of MIF-AS1

To identify the target and potential mechanism of MIF-AS1 in NSCLC chemo- and radio-resistance, the mRNA targets of MIF-AS1 were identified by a ceRNA network. Using the miRWalk and NPInterv4 databases, we first identified 626 miRNAs targeted by the 5189 differentially expressed lncRNAs between the sensitive and resistant groups of NSCLC patients. We then used the multiMiR package to identify the targeted mRNAs of these 626 miRNAs, and 1650 targeted mRNAs were ultimately obtained. Next, we performed enrichment analysis of these target genes. GO enrichment analysis revealed that these genes were mostly enriched in protein modification, DNA-binding-related, and ubiquitin-binding-related functions (Fig. 4A). KEGG pathway enrichment analysis revealed that these genes were enriched in the PI3K-Akt signaling pathway, the MAPK signaling pathway, and the tumor-associated pathways (Fig. 4B). Furthermore, based on the identified MIF-AS1-targeted miRNAs, mRNAs, and enriched KEGG pathways, we constructed a ceRNA network. This network revealed several key genes targeted by MIF-AS1, including ACVR1B, EHD2, RAD21, EPAS1, and FGF9 (Fig. 4C). Using the TCGA database, we analyzed the correlation of MIF-AS1 with ACVR1B, EHD2, RAD21, EPAS1, and FGF9 in NSCLC, and found that MIF-AS1 expression was positively correlated with RAD21 expression only (Fig. 4D). RT-qPCR and western blot analyses demonstrated that knockdown of MIF-AS1 resulted in reduced RAD21 expression in NSCLC cells (Fig. 4E). Next, we analyzed the effect of RAD21 on NSCLC prognosis, and found

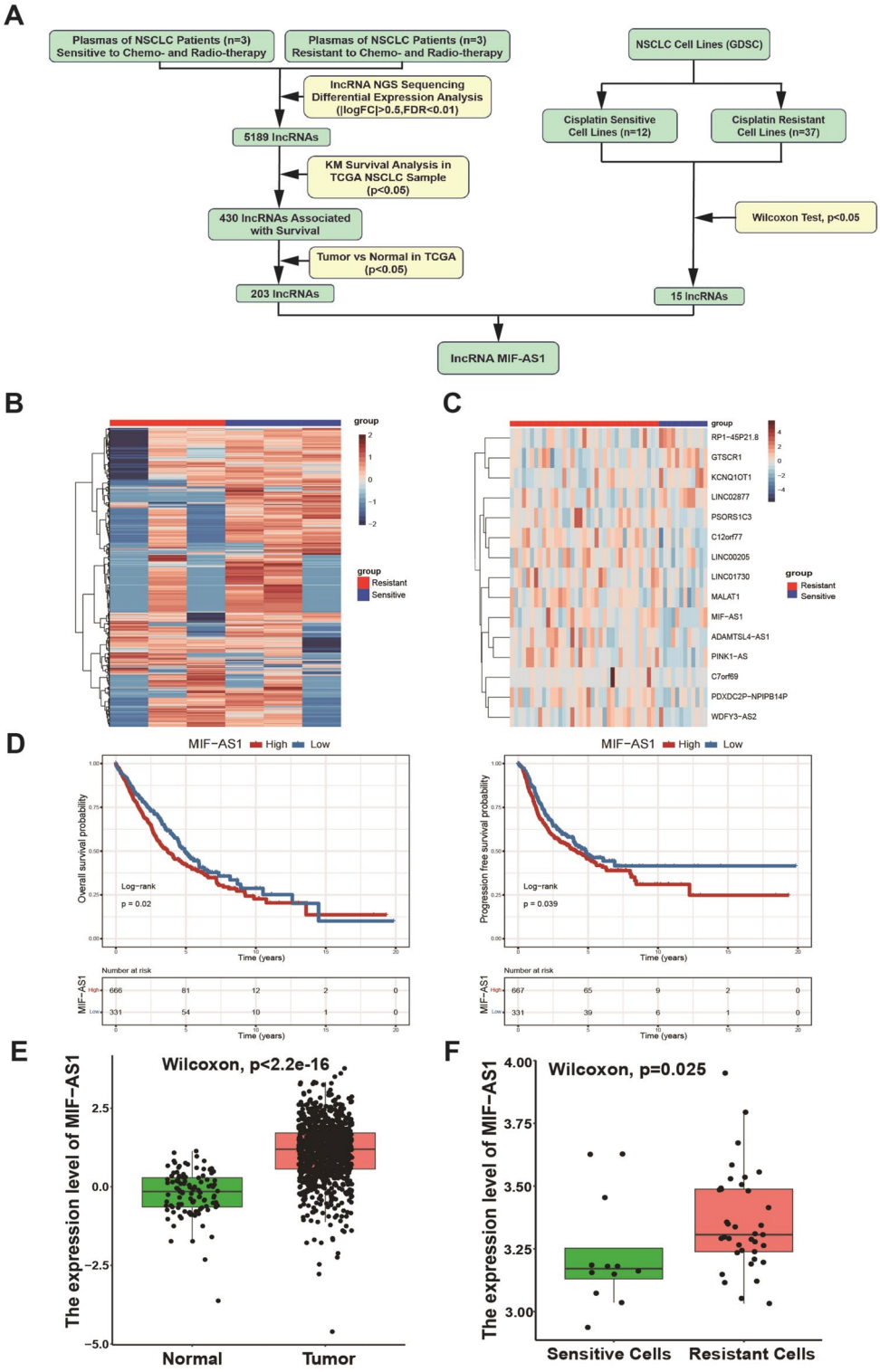

Fig. 1. (**A**) The flowchart describes the identification of the lncRNA MIF-AS1. (**B**) Heatmap showing the 203 differentially expressed plasma lncRNAs between the sensitive and resistant NSCLC patients. (**C**) Heatmap showing the 15 differentially expressed lncRNAs between cisplatin-sensitive and resistant NSCLC cell lines. (**D**) KM survival analysis showing that high expression of MIF-AS1 is associated with poor overall survival and progression-free survival of NSCLC patients. (**E**) The expression of MIF-AS1 is higher in NSCLC tumors than in normal tissues (Wilcoxon test). (**F**) The expression of MIF-AS1 is higher in cisplatin-resistant NSCLC cell lines than in cisplatin-sensitive NSCLC cell lines (Wilcoxon test).

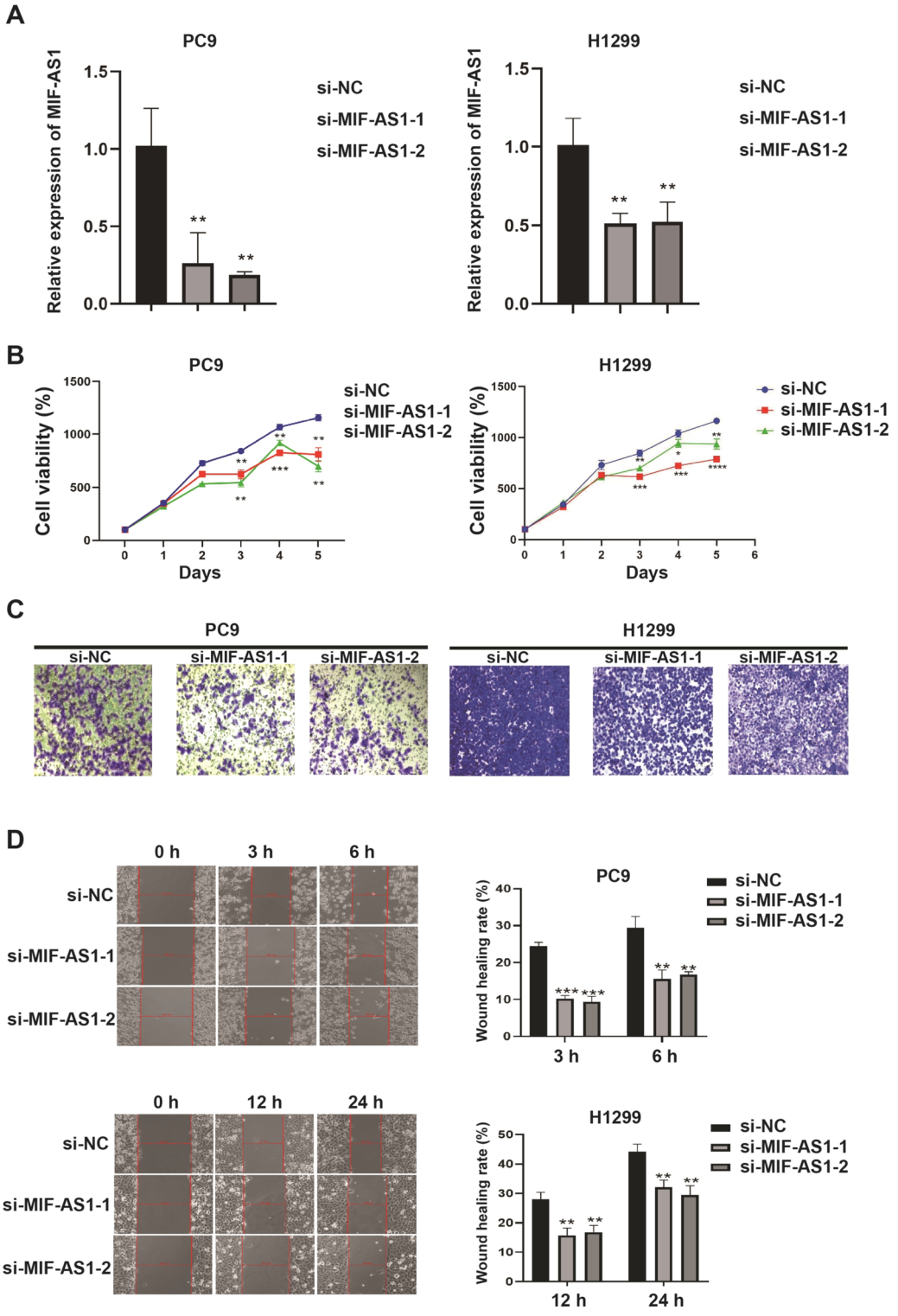

Fig. 2. (**A**) RT-qPCR showing the knockdown of MIF-AS1 by siRNA in PC9 and H1299 NSCLC cells (one-way ANOVA followed by Dunnett's post hoc test). (**B**) Knockdown of MIF-AS1 significantly decreases the viability of PC9 and H1299 NSCLC cells (one-way ANOVA followed by Dunnett's post hoc test). (**C**) Knockdown of MIF-AS1 attenuates the invasion of NSCLC cells. After PC9 and H1299 NSCLC cells were transfected with MIF-AS1 siRNA and control siRNA, the invasion ability of the cells was evaluated by Matrigel invasion assay. (**D**) Knockdown of MIF-AS1 attenuates the mobility of NSCLC cells. After PC9 and H1299 NSCLC cells were transfected with MIF-AS1 siRNA and control siRNA, the migration ability of cells was evaluated by cell scratch assay (one-way ANOVA followed by Dunnett's post hoc test).

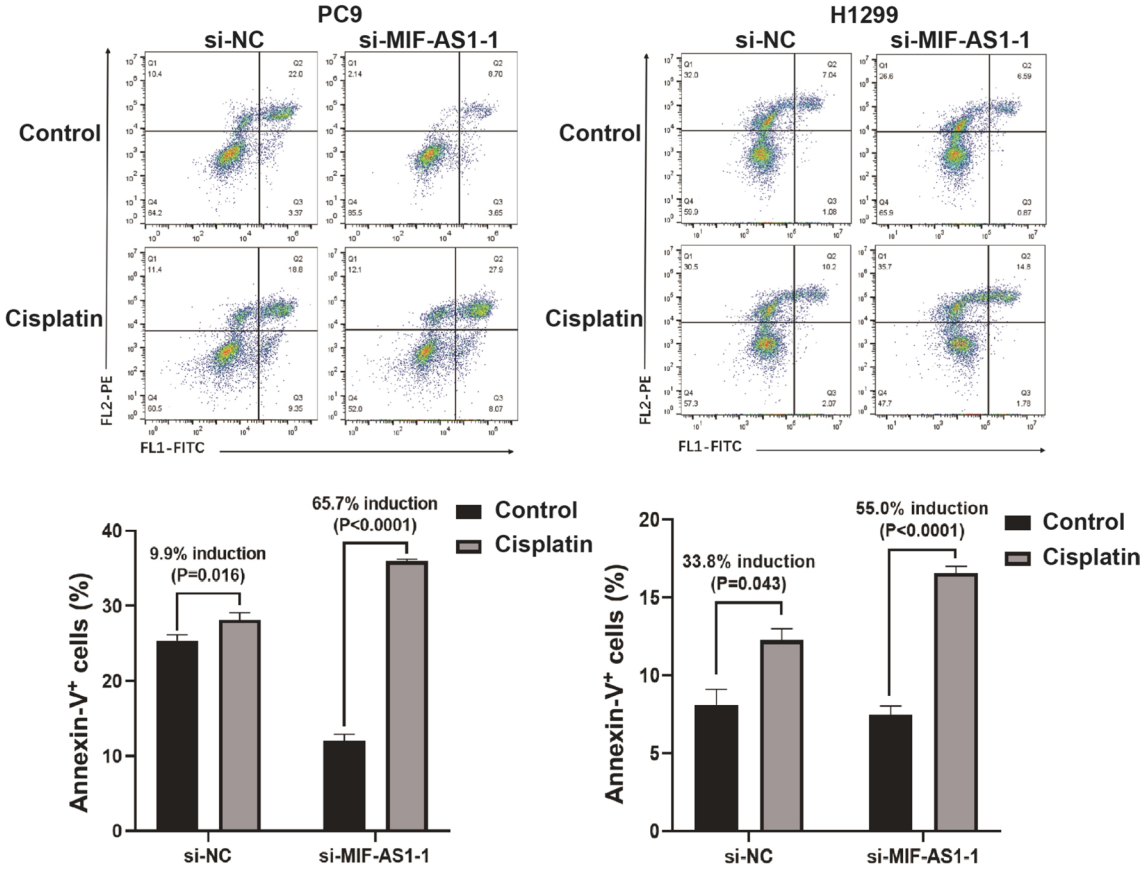

Fig. 3. MIF-AS1 knockdown enhances cisplatin-induced apoptosis in NSCLC cells. PC9 and H1299 cells were transiently transfected with MIF-AS1 siRNA and control siRNA for 48 h, and then the transfected cells were treated with cisplatin (10 μg/mL) for 24 h. After treatment, apoptosis was detected by Annexin V apoptosis assay (Student's t test).

that higher expression of RAD21 was significantly associated with worse survival (Fig. 4F). The function of RAD21 is involved in DNA damage repair[20]. Therefore, these results indicate that the level of MIF-AS1 shows a significant positive correlation with RAD21 expression in NSCLC, implying that MIF-AS1/RAD21 axis may promote chemo- and radio-resistance by enhancing DNA damage repair.

The ability of the lncRNA MIF-AS1 to predict the response of NSCLC to chemo- and radio-therapy

To determine whether plasma MIF-AS1 level had a predictive potential on the response of chemo- and radio-therapy in NSCLC, we collected the plasma of 124 NSCLC patients before chemo- and radio-treatment (Fig. 5A and Table S3). The RT-qPCR results indicated that the expression level of MIF-AS1 in the chemo- and radio-resistant group was significantly elevated, compared with the sensitive group in NSCLC (Fig. 5B). ROC curve analysis indicated that MIF-AS1 had a moderate discriminatory ability for predicting the response to chemo- and radio-therapy in NSCLC, with an AUC value of 0.724 (95% CI = 0.609 to 0.839), a sensitivity of 77.3%, and a specificity of 63.7% (Fig. 5C). Previous study has shown that carcinoembryonic antigen (CEA) was used for assessment of therapy response in NSCLC[22]. However, the corresponding AUC value of the conventional tumor biomarker CEA for discriminating sensitive NSCLC patients from resistant NSCLC patients was only 0.556 (95% CI = 0.437 to 0.715, sensitivity = 61.9%, specificity = 63.7%) (Fig. 5D). In addition, clinical data from 124 NSCLC patients were collected and analyzed to explore the relationships between MIF-AS1 expression and clinicopathological characteristics. As indicated in Table 1, MIF-AS1 expression was not significantly associated with age, sex, smoking status, tumor size, tumor stage, lymph node metastasis or remote metastasis ($p > 0.05$). This study demonstrates that the lncRNA MIF-AS1 is superior to the conventional biomarker CEA for predicting the response of NSCLC to chemo- and radio-therapy.

The ability of MIF-AS1 combined with radiomics to predict the response of NSCLC to chemo- and radio-therapy

To determine whether the MIF-AS1 level combined with radiomics had a better predictive ability, we collected the chest CT images and MIF-AS1 expression levels of 38 NSCLC patients from the TCGA (Table S4). First, we segmented the tumor areas in each layer of the CT images. The tumor areas were manually outlined using AccuContour software 3.1 (Manteia, Fujian, China), and then reconstructed in three dimensions. A total of

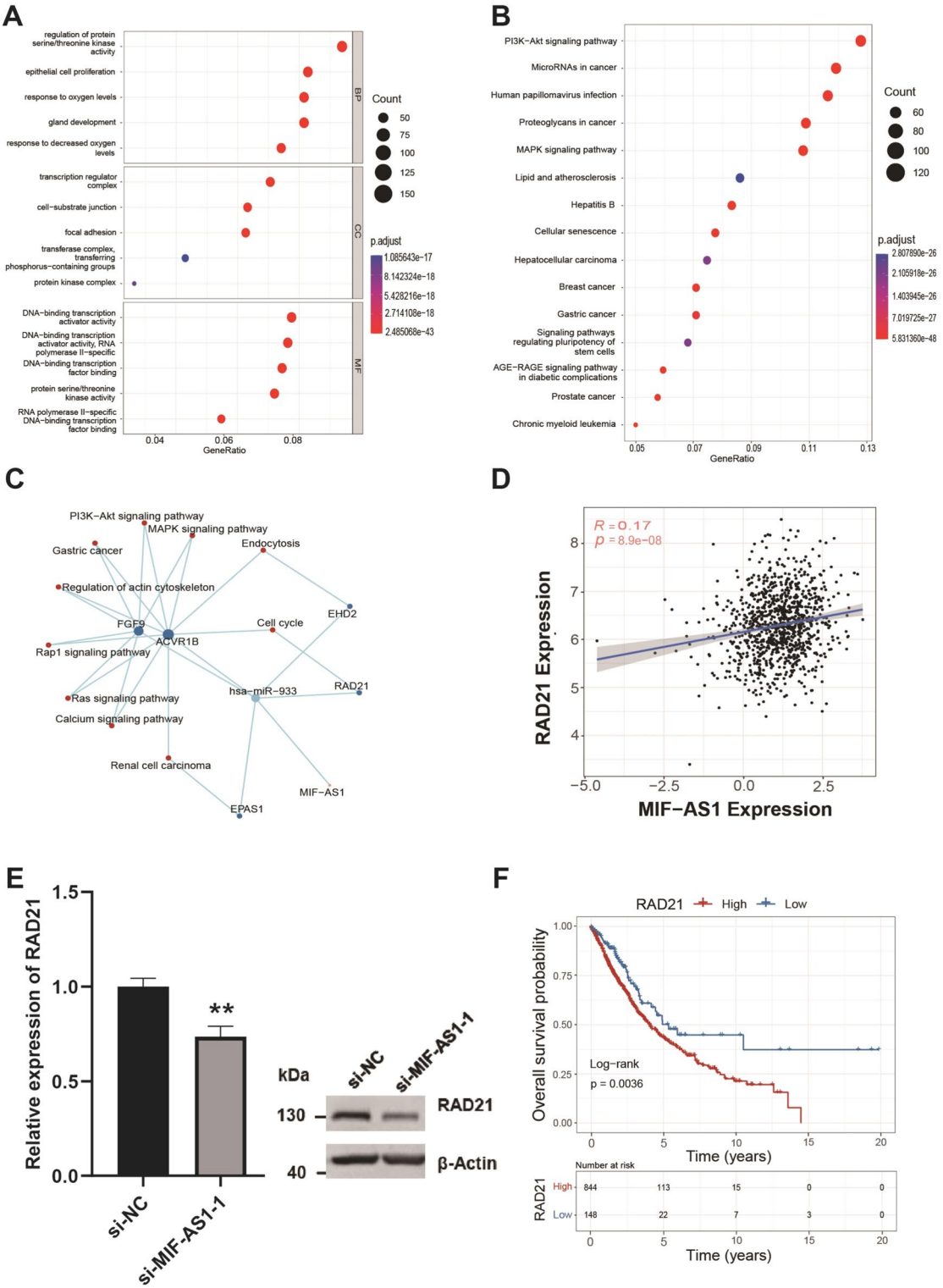

Fig. 4. (**A**) GO enrichment analysis of 1650 targeted mRNAs. (**B**) KEGG pathway enrichment analysis of 1650 targeted mRNAs[21]. (**C**) The ceRNA network map of MIF-AS1. (**D**) Analysis of the correlation between MIF-AS1 expression and RAD21 expression in NSCLC tumors from the TCGA database (Pearson correlation analysis). (**E**) Knockdown of MIF-AS1 by siRNA decreases RAD21 expression in NSCLC PC9 cells. PC9 cells were transfected with control (si-NC) and MIF-AS1 siRNAs (si-MIF-AS1-1), and the mRNA and protein levels of RAD21 were determined by qPCR and western blot (Student's t test). (**F**) KM survival analysis of RAD21 in the TCGA dataset. NSCLC patients were divided into low-expression and high-expression groups based on the optimal cut-off point.

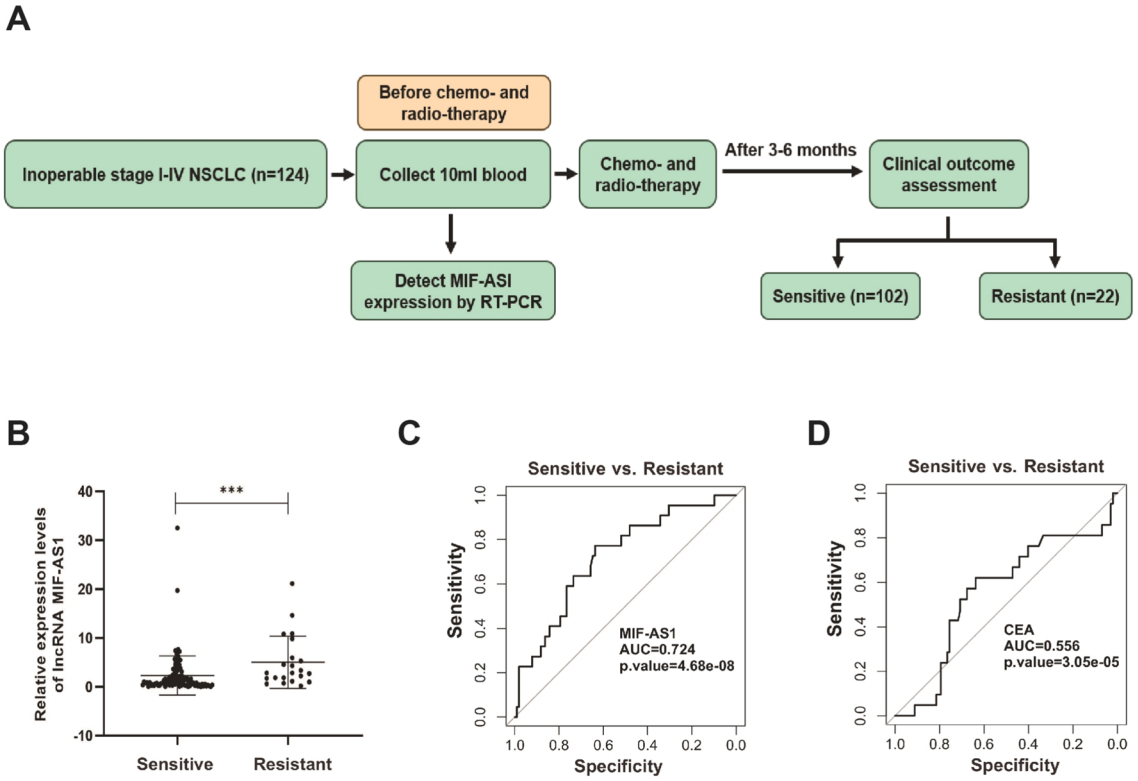

Fig. 5. (**A**) Schematic diagram describing the patient enrollment and study workflow. (**B**) Plasma MIF-AS1 levels in 124 NSCLC patients who were chemo- and radio-sensitive or resistant (Mann–Whitney U test). (**C**) ROC curve analysis of the predictive value of MIF-AS1 for the response to chemo- and radio-therapy in 124 NSCLC patients. (**D**) ROC curve analysis of the predictive value of CEA for the response to chemo- and radio-therapy in 124 NSCLC patients.

1409 different radiomic features were extracted from the tumor simulation images (Fig. 6A). LASSO regression algorithm was used to select the radiomic features that were associated with the response to chemo- and radio-therapy (Fig. 6B). LASSO regression identified two radiomic features, "correlation" and "mean", that were associated with the response to chemo- and radio-therapy. The Z-score of "correlation" feature was significantly higher in the sensitive group, whereas the Z-score of "mean" feature was significantly higher in the resistant group (Fig. 6C).

Using two radiomic features and MIF-AS1 expression data, we developed a predictive model for radio- and chemo-therapy response via multivariate logistic regression, which was presented as a nomogram. (Fig. 6D). We then assessed the model's predictive performance using ROC curve analysis. In the TCGA training dataset, the model demonstrated strong predictive performance, achieving an AUC of 0.886 (Fig. 6E). In the independent validation set, we collected chest CT images of 124 NSCLC patients from Hefei Cancer Hospital of CAS. Plasmas MIF-AS1 levels were available for these NSCLC patients. Using the nomogram of MIF-AS1 combined with the two radiomic features, the AUC for predicting the response to chemo- and radio-therapy was 0.808 (Fig. 6F), indicating better discriminative ability than the plasma MIF-AS1 level alone (AUC = 0.724).

The Sankey diagram illustrates a good stratification of NSCLC patients in the training and validation datasets according to the model's classification (Fig. 7A). Finally, decision curve analysis (DCA) was performed to evaluate the clinical utility of the nomogram, which incorporated radiomic features and MIF-AS1 levels. As shown in Fig. 7B, the nomogram consistently yielded a higher net benefit across a wide range of threshold probabilities than both the treat-all and treat-none strategies in the training and validation sets. These results support the potential clinical utility of the model in aiding clinical decision-making.

Discussion

In this study, by an integrated bioinformatics analysis, we identified plasma lncRNA MIF-AS1, whose level was significantly higher in the chemo- and radio-resistant NSCLC patients. Analysis of ROC curves demonstrated that plasma MIF-AS1 exhibits superior diagnostic performance (AUC = 0.724) over the conventional biomarker CEA (AUC = 0.556) in predicting response to chemo- and radio-therapy in NSCLC. Furthermore, we developed a combined model incorporating MIF-AS1 and radiomic features, which demonstrated superior predictive performance for treatment response in NSCLC, achieving an AUC of 0.808.

Our study revealed that MIF-AS1 promoted tumor cell proliferation, migration and invasion in NSCLC. This is consistent with its significant up-regulation in various other malignancies, such as ovarian, gastric, and breast cancer. MIF-AS1 expression was significantly elevated in ovarian cancer tissues and was associated with a poor

Parameters	Patients (number)	Plasma MIF-AS1 level [median (interquartile spacing)]	*P* value
Patients	124	1.22 (0.56–3.31)	
Age			0.73
≤ 60	35	1.35 (0.50–4.81)	
> 60	89	1.20 (0.60–2.87)	
Gender			0.37
Male	94	1.26 (0.53–3.69)	
Female	30	1.02 (0.55–2.77)	
Smoking status			0.68
Yes	57	1.14 (0.46–3.60)	
No	67	1.23 (0.71–2.97)	
Tumor size			0.75
≤ 3 cm	78	1.31 (0.52–3.57)	
> 3 cm	46	1.11 (0.59–2.13)	
Stage			0.71
Ⅰ - Ⅱ	20	1.15 (0.65–3.99)	
Ⅲ-Ⅳ	104	1.26 (0.56–3.17)	
Lymph node metastasis			0.29
Yes	89	1.55 (0.59–3.64)	
No	35	1.05 (0.48–2.36)	
Distal metastasis			0.85
Yes	68	1.29 (0.58–3.29)	
No	56	1.16 (0.45–3.71)	
Tumor pathology			0.56
LUAD	74	1.48 (0.52–3.34)	
LUSC	50	1.13 (0.62–2.79)	

Table 1. Correlation analysis between plasma MIF-AS1 levels and clinicopathological indicators in NSCLC patients. *LUAD* Lung adenocarcinoma; *LUSC* Lung squamous cell carcinoma

prognosis. Functionally, the downregulation of MIF-AS1 in ovarian cancer cells markedly inhibited cellular proliferation, migration, and invasion[23]. Ni et al. reported that the MIF-AS1 polymorphism rs755622 (TC/CC variants) was associated with elevated MIF-AS1 expression in both normal and gastric cancer tissues, conferring a poorer survival in gastric cancer patients compared to those with the TT genotype[24]. Similarly, MIF-AS1 was upregulated in breast cancer and correlated with adverse patient outcomes. Moreover, a ceRNA network (MIF-AS1/miR-624-3p/HOXB8) was identified to contribute to the development of breast cancer[25]. Taken together, these findings underscore the oncogenic significance of MIF-AS1, thereby establishing its dual promise as a biomarker and therapeutic target in oncology.

Our study identified RAD21 as a potential target of MIF-AS1. The RAD21 gene encodes a protein critical for DNA double-strand break repair and apoptosis regulation. As a core subunit of the cohesin complex, it is essential for sister chromatid cohesion[26]. The cohesin complex ensures proper chromosome segregation, facilitates post-replicative DNA repair, and prevents inappropriate recombination[27,28]. LncRNAs can modulate the expression of cohesins and their subunits. Since the cohesin complex plays a pivotal role in maintaining genomic stability, its dysregulation by lncRNAs constitutes a key mechanism in tumorigenesis[29]. Wang et al. have indicated that RAD21 expression was upregulated in ionizing radiation-insensitive hepatocellular carcinoma tissues, and its overexpression attenuated ionizing radiation-induced DNA damage in hepatocellular carcinoma cells[20]. In breast cancer, RAD21 was identified as a gene associated with response to tamoxifen treatment[30,31]. Furthermore, inhibition of RAD21 expression reduced cell growth and enhanced the cytotoxicity of etoposide and bleomycin in human breast cancer cells[32]. In NSCLC, RAD21 overexpression mediated cisplatin resistance through enhanced DNA damage repair[33]. Therefore, our study demonstrates that MIF-AS1 knockdown sensitizes NSCLC cells to cisplatin-induced apoptosis, an effect likely mediated by reduced RAD21 expression.

The quantifiable deep tumor features on CT images exhibit potential for predicting therapy response. Trebeschi et al. developed a radiomic biomarker for evaluating immunotherapy response in NSCLC, which achieved an AUC of 0.83. This model shows potential for improving patient stratification in both neoadjuvant and palliative care[34]. Li et al. demonstrated that a model integrating radiomic and clinicopathological features achieved AUCs of 0.762 and 0.814 for predicting PD-L1 expression levels exceeding 1% and 50%, respectively. This indicates that such a model can effectively identify NSCLC patients likely to respond to PD-L1 immunotherapy[35]. Wang et al. identified three CT radiomic features associated with tumor mutation burden (TMB) in NSCLC. Based on these features, they developed a model for predicting both TMB levels and immunotherapy response[36]. Lin et al. demonstrated that integrating two plasma miRNA biomarkers with a radiological characteristic could more accurately identify lung cancer in patients with indeterminate pulmonary nodules[37]. Xing et al. demonstrated that integrating three DNA methylation biomarkers (PTGER4, RASSF1A, and SHOX2) with one

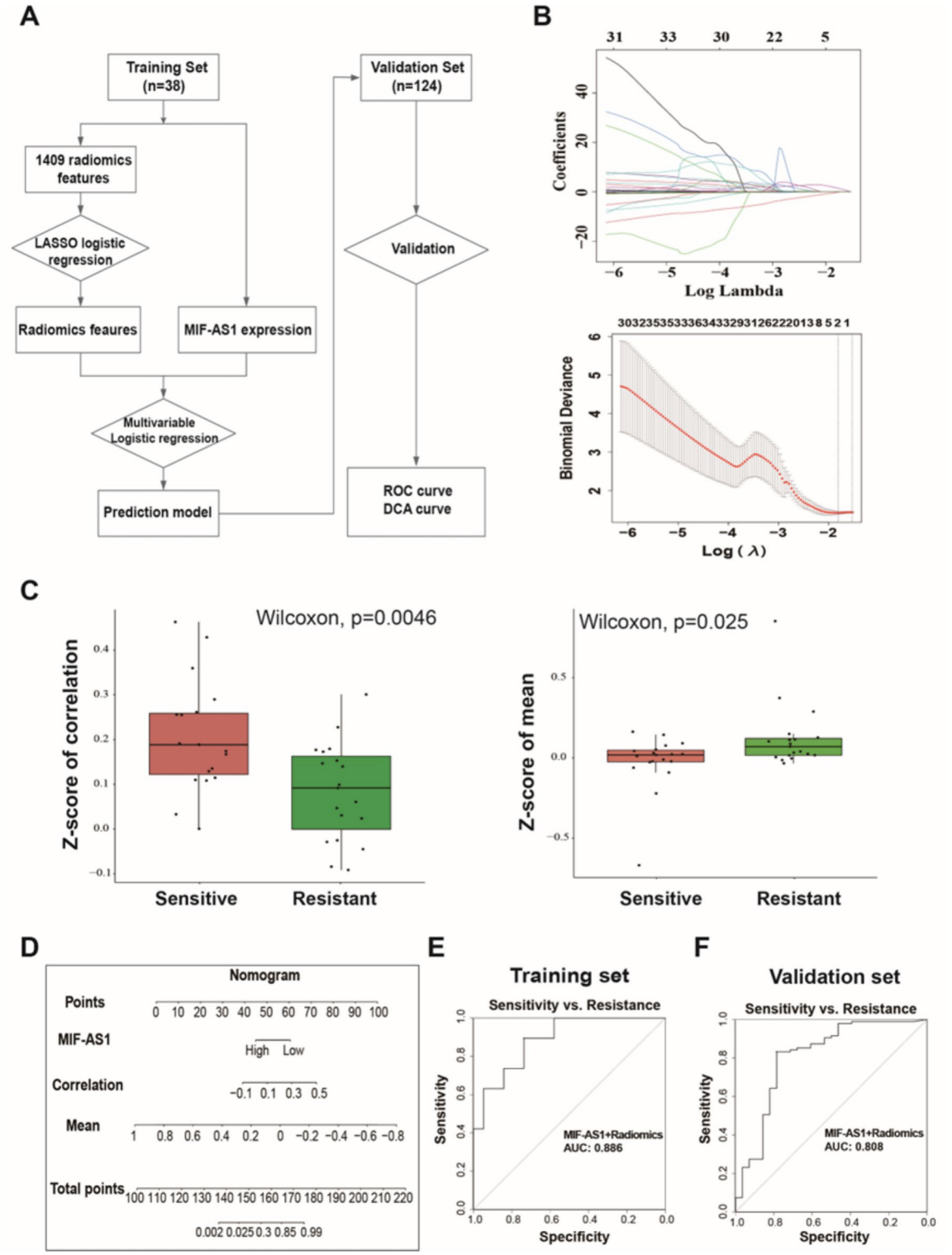

Fig. 6. (**A**) Study workflow for the predictive model based on radiomic features and MIF-AS1 levels. (**B**) LASSO regression identified two radiomic features (correlation and mean) associated with chemo- and radio-therapy response. The coefficient profile of the model (upper panel) and the tuning parameter (λ) selected via tenfold cross-validation (lower panel) are presented. (**C**) Z-score values of the two radiomics features (correlation and mean) in NSCLC patients who were sensitive and resistant to chemo- and radio-therapy (Wilcoxon test). (**D**) A dynamic nomogram was constructed using the two radiomic features (correlation and mean) and the MIF-AS1 level. (**E**) ROC curve of the nomogram based on two radiomic features (correlation and mean) and the MIF-AS1 level to predict chemo- and radio-therapy response in the TCGA training set. (**F**) ROC curve of the nomogram based on two radiomics features (correlation and mean) and the MIF-AS1 level to predict chemo- and radio-chemotherapy response in the validation set of 124 NSCLC patients from the Hefei Cancer Hospital of CAS.

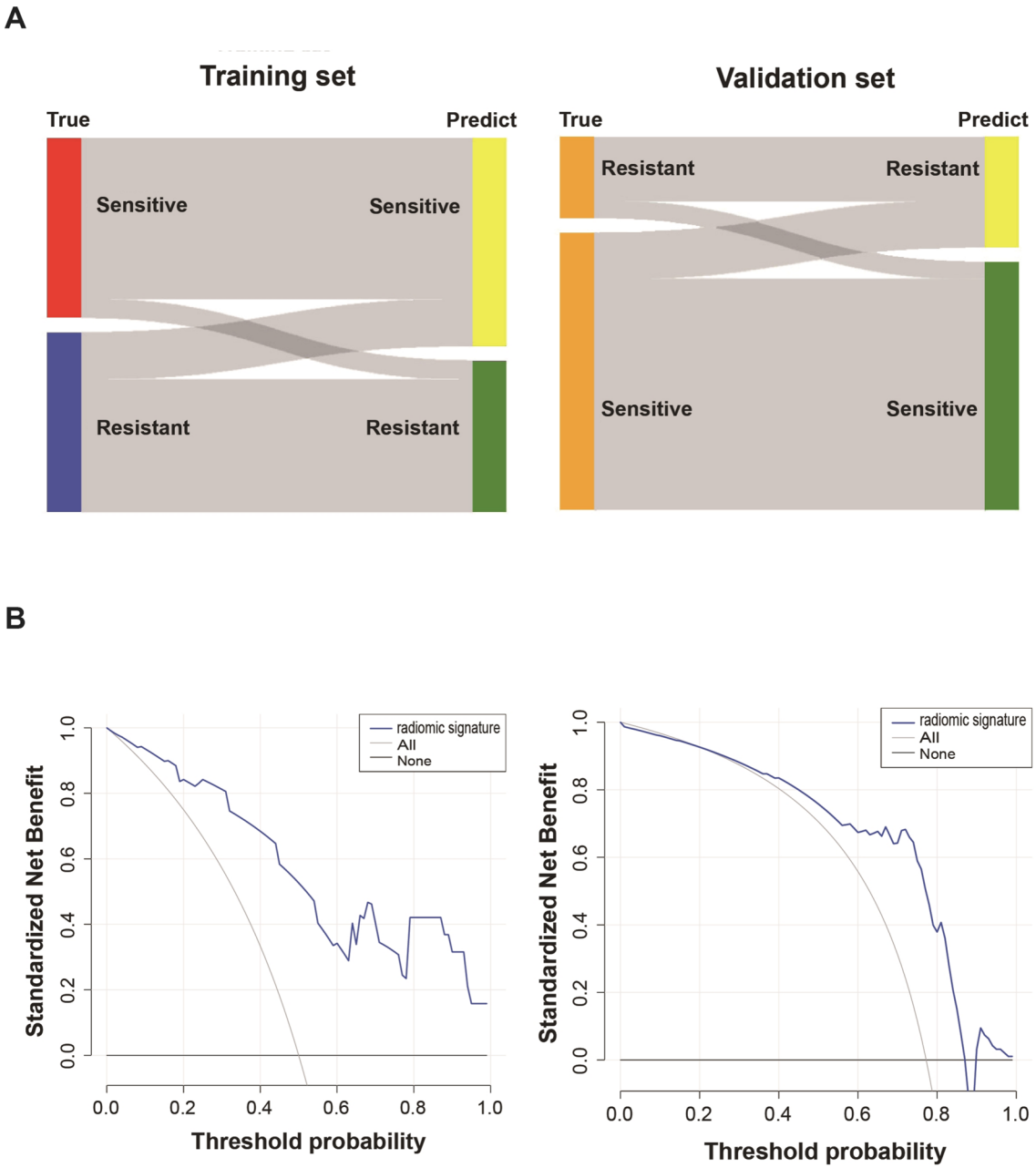

Fig. 7. (**A**) Sankey diagram of patient classification by the prediction model (correct vs. incorrect) in the training and validation datasets. (**B**) Decision curve analysis (DCA) of the prediction model, showing the net benefit against the threshold probability.

radiological characteristic could more accurately identify lung cancer in patients with CT-detected pulmonary nodules[38]. Therefore, our and previous studies demonstrate that integrating plasma biomarkers with radiological characteristics holds promise for developing more accurate predictive models in cancer diagnosis and prognosis.

Nevertheless, the current study has several limitations. Firstly, the sample collection was confined to a single institution, and the cohort size was relatively small, which may constrain the broad applicability of the model. The clinical application of the MIF-AS1 and radiomics-based model warrants further investigation through prospective, multicenter studies with larger sample sizes. Second, the functional validation of MIF-AS1 was conducted in vitro using lung adenocarcinoma cell lines. A notable limitation is the absence of validation in lung squamous cell carcinoma cell lines. Furthermore, the precise molecular mechanisms through which MIF-AS1 contributes to NSCLC progression and therapy resistance remain to be elucidated.

Conclusions

In summary, our study identifies MIF-AS1 as a promising biomarker for predicting chemo- and radio-therapy response in NSCLC. Furthermore, the predictive model integrating CT radiomics with MIF-AS1 levels demonstrates enhanced accuracy for stratifying patient response.

Data availability

The raw sequence data of exosomal lncRNAs reported in this paper have been deposited in the Genome Sequence Archive in National Genomics Data Center, China National Center for Bioinformation/Beijing Institute of Genomics, Chinese Academy of Sciences (GSA-Human: HRA014950) that are publicly accessible at https://ngdc.cncb.ac.cn/gsa-human.

Code availability

Not applicable.

Received: 11 November 2025; Accepted: 5 February 2026
Published online: 11 February 2026

References

1. Chen, Y., Zitello, E., Guo, R. & Deng, Y. The function of LncRNAs and their role in the prediction, diagnosis, and prognosis of lung cancer. *Clin. Transl. Med.* **11**, e367. https://doi.org/10.1002/ctm2.367 (2021).
2. Lin, Y., Leng, Q., Zhan, M. & Jiang, F. A Plasma Long Noncoding RNA Signature for Early Detection of Lung Cancer. *Translational oncology* **11**, 1225–1231. https://doi.org/10.1016/j.tranon.2018.07.016 (2018).
3. Deans, A. J. & West, S. C. DNA interstrand crosslink repair and cancer. *Nat. Rev. Cancer* **11**, 467–480. https://doi.org/10.1038/nrc3088 (2011).
4. Chen, Z. et al. Long non-coding RNA in lung cancer. *Clinica chimica acta Int. J. Clin. Chem.* **504**, 190–200. https://doi.org/10.1016/j.cca.2019.11.031 (2020).
5. Liu, H. Y. et al. lncRNA SLC16A1-AS1 as a novel prognostic biomarker in non-small cell lung cancer. *J. Investigative Med. : Official Publication of the Am. Federation for Clin. Res.* **68**, 52–59. https://doi.org/10.1136/jim-2019-001080 (2020).
6. Liu, G. et al. Expression and significance of LncRNA MNX1-AS1 in non-small cell lung cancer. *Onco. Targets. Ther.* **12**, 3129–3138. https://doi.org/10.2147/ott.S198014 (2019).
7. Zhang, X. et al. Role of non-coding RNAs and RNA modifiers in cancer therapy resistance. *Mol. Cancer* **19**, 47. https://doi.org/10.1186/s12943-020-01171-z (2020).
8. Guiducci, G. & Stojic, L. Long Noncoding RNAs at the Crossroads of Cell Cycle and Genome Integrity. *Trends in genetics : TIG* **37**, 528–546. https://doi.org/10.1016/j.tig.2021.01.006 (2021).
9. Sun, W., Zu, Y., Fu, X. & Deng, Y. Knockdown of lncRNA-XIST enhances the chemosensitivity of NSCLC cells via suppression of autophagy. *Oncol. Rep.* **38**, 3347–3354. https://doi.org/10.3892/or.2017.6056 (2017).
10. Zhang, M. et al. Long Noncoding RNA CRNDE/PRC2 Participated in the Radiotherapy Resistance of Human Lung Adenocarcinoma Through Targeting p21 Expression. *Oncol. Res.* **26**, 1245–1255. https://doi.org/10.3727/096504017x14944585873668 (2018).
11. Liu, L. et al. Long non-coding RNA ANRIL promotes homologous recombination-mediated DNA repair by maintaining ATR protein stability to enhance cancer resistance. *Mol. Cancer* **20**, 94. https://doi.org/10.1186/s12943-021-01382-y (2021).
12. Tamang, S. et al. SNHG12: An LncRNA as a Potential Therapeutic Target and Biomarker for Human Cancer. *Front. Oncol.* **9**, 901. https://doi.org/10.3389/fonc.2019.00901 (2019).
13. Li, C. et al. Tumor-derived exosomal lncRNA GAS5 as a biomarker for early-stage non-small-cell lung cancer diagnosis. *J. Cell. Physiol.* **234**, 20721–20727. https://doi.org/10.1002/jcp.28678 (2019).
14. Nagasaka, M. et al. Liquid biopsy for therapy monitoring in early-stage non-small cell lung cancer. *Mol. Cancer* **20**, 82. https://doi.org/10.1186/s12943-021-01371-1 (2021).
15. Lin, L. Y. et al. Tumor-originated exosomal lncUEGC1 as a circulating biomarker for early-stage gastric cancer. *Mol. Cancer* **17**, 84. https://doi.org/10.1186/s12943-018-0834-9 (2018).
16. Min, L. et al. Exosomal LncRNA RP5-977B1 as a novel minimally invasive biomarker for diagnosis and prognosis in non-small cell lung cancer. *Int. J. Clin. Oncol.* **27**, 1013–1024. https://doi.org/10.1007/s10147-022-02129-5 (2022).
17. Cucchiara, F. et al. Combining liquid biopsy and radiomics for personalized treatment of lung cancer patients State of the art and new perspectives. *Pharmacological Res.* **169**, 105643. https://doi.org/10.1016/j.phrs.2021.105643 (2021).
18. Wen, Q., Yang, Z., Dai, H., Feng, A. & Li, Q. Radiomics Study for Predicting the Expression of PD-L1 and Tumor Mutation Burden in Non-Small Cell Lung Cancer Based on CT Images and Clinicopathological Features. *Front. Oncol.* **11**, 620246. https://doi.org/10.3389/fonc.2021.620246 (2021).
19. He, B., Dong, D., She, Y., Zhou, C., Fang, M., Zhu, Y., Zhang, H., Huang, Z., Jiang, T., Tian, J.; *et al.* Predicting response to immunotherapy in advanced non-small-cell lung cancer using tumor mutational burden radiomic biomarker. *Journal for immunotherapy of cancer* **2020**, *8*, https://doi.org/10.1136/jitc-2020-000550.
20. Wang, J. et al. MiR-320b/RAD21 axis affects hepatocellular carcinoma radiosensitivity to ionizing radiation treatment through DNA damage repair signaling. *Cancer Sci.* **112**, 575–588. https://doi.org/10.1111/cas.14751 (2021).
21. Kanehisa, M. & Goto, S. KEGG: kyoto encyclopedia of genes and genomes. *Nucleic Acids Res.* **28**, 27–30. https://doi.org/10.1093/nar/28.1.27 (2000).
22. Holdenrieder, S. et al. Carcinoembryonic antigen and cytokeratin-19 fragments for assessment of therapy response in non-small cell lung cancer: a systematic review and meta-analysis. *Br. J. Cancer* **116**, 1037–1045. https://doi.org/10.1038/bjc.2017.45 (2017).
23. Fan, Y. et al. LncRNA MIF-AS1 aggravates the progression of ovarian cancer by sponging miRNA-31-5p. *Eur. Rev. Med. Pharmacol. Sci.* **24**, 2248–2255. https://doi.org/10.26355/eurrev_202003_20490 (2020).
24. Ni, P. et al. Correlation of MIF-AS1 polymorphisms with the risk and prognosis of gastric cancer. *Pathol. Res. Pract.* **233**, 153850. https://doi.org/10.1016/j.prp.2022.153850 (2022).
25. Ding, J., Wu, W., Yang, J. & Wu, M. Long non-coding RNA MIF-AS1 promotes breast cancer cell proliferation, migration and EMT process through regulating miR-1249-3p/HOXB8 axis. *Pathol. Res. Pract.* **215**, 152376. https://doi.org/10.1016/j.prp.2019.03.005 (2019).
26. Nasmyth, K. & Haering, C. H. Cohesin: its roles and mechanisms. *Annu. Rev. Genet.* **43**, 525–558. https://doi.org/10.1146/annurev-genet-102108-134233 (2009).
27. Nishiyama, T. Cohesion and cohesin-dependent chromatin organization. *Curr. Opin. Cell Biol.* **58**, 8–14. https://doi.org/10.1016/j.ceb.2018.11.006 (2019).
28. Perea-Resa, C., Wattendorf, L., Marzouk, S. & Blower, M. D. Cohesin: behind dynamic genome topology and gene expression reprogramming. *Trends Cell Biol.* **31**, 760–773. https://doi.org/10.1016/j.tcb.2021.03.005 (2021).

29. Kuru-Schors, M., Haemmerle, M. & Gutschner, T. The Cohesin Complex and Its Interplay with Non-Coding RNAs. *Non-coding RNA* **2021**, *7*, https://doi.org/10.3390/ncrna7040067.
30. van Agthoven, T. et al. Selective recruitment of breast cancer anti-estrogen resistance genes and relevance for breast cancer progression and tamoxifen therapy response. *Endocr. Relat. Cancer* **17**, 215–230. https://doi.org/10.1677/erc-09-0062 (2010).
31. Mendes-Pereira, A. M. et al. Genome-wide functional screen identifies a compendium of genes affecting sensitivity to tamoxifen. *Proc. Natl. Acad. Sci. U.S.A.* **109**, 2730–2735. https://doi.org/10.1073/pnas.1018872108 (2012).
32. Atienza, J. M. et al. Suppression of RAD21 gene expression decreases cell growth and enhances cytotoxicity of etoposide and bleomycin in human breast cancer cells. *Mol. Cancer Ther.* **4**, 361–368. https://doi.org/10.1158/1535-7163.Mct-04-0241 (2005).
33. Zhao, J. et al. The regulatory and predictive functions of miR-17 and miR-92 families on cisplatin resistance of non-small cell lung cancer. *BMC Cancer* **15**, 731. https://doi.org/10.1186/s12885-015-1713-z (2015).
34. Trebeschi, S. et al. Predicting response to cancer immunotherapy using noninvasive radiomic biomarkers. *Annals Oncology : official J. Eur. Soc. Med. Oncology* **30**, 998–1004. https://doi.org/10.1093/annonc/mdz108 (2019).
35. Li, J., Ge, S., Sang, S., Hu, C. & Deng, S. Evaluation of PD-L1 Expression Level in Patients With Non-Small Cell Lung Cancer by (18)F-FDG PET/CT Radiomics and Clinicopathological Characteristics. *Front. Oncol.* **11**, 789014. https://doi.org/10.3389/fonc.2021.789014 (2021).
36. Wang, J. et al. CT radiomics-based model for predicting TMB and immunotherapy response in non-small cell lung cancer. *BMC Med. Imaging* **24**, 45. https://doi.org/10.1186/s12880-024-01221-8 (2024).
37. Lin, Y. et al. A classifier integrating plasma biomarkers and radiological characteristics for distinguishing malignant from benign pulmonary nodules. *Int. J. Cancer* **141**, 1240–1248. https://doi.org/10.1002/ijc.30822 (2017).
38. Xing, W. et al. A prediction model based on DNA methylation biomarkers and radiological characteristics for identifying malignant from benign pulmonary nodules. *BMC Cancer* **21**, 263. https://doi.org/10.1186/s12885-021-08002-4 (2021).

Acknowledgements

This study was supported by the National Natural Science Foundation of China (81872438), the Program of Research and Development of Key Common Technologies and Engineering of Major Scientific and Technological Achievements in Hefei (2021YL007), the Collaborative Innovation Program of Hefei Science Center, CAS (2022HSC-CIP015), and the Program of Clinical Medical Translational Research in Anhui Province (202304295107020092).

Author contributions

HW and BH designed the study. FY, JY, YY, ZH, HJ, YZ (Yucheng Zhang) and YZ (Yani Zhang) collected the samples and performed the in vitro experiments. FY, JW (Jiexiao Wang), JW (Jialiang Wang), QZ and JQ performed the bioinformatics analysis. FY and JZ wrote the first draft of the manuscript. BH and HW revised the manuscript. All authors reviewed the final manuscript.

Funding

This study was supported by the National Natural Science Foundation of China (81872438), the Program of Research and Development of Key Common Technologies and Engineering of Major Scientific and Technological Achievements in Hefei (2021YL007), the Collaborative Innovation Program of Hefei Science Center, CAS (2022HSC-CIP015), and the Program of Clinical Medical Translational Research in Anhui Province (202304295107020092).

Declarations

Competing interests

The authors declare no competing interests.

Ethical approval

The study was approved by The Ethics Committee of Hefei Cancer Hospital of the Chinese Academy of Sciences, with the approval number SL-PJ2023-098.

Consent to participate

All clinical samples and information were obtained with written informed consent of the patients.

Consent for publication

Not applicable.

Additional information

Supplementary Information The online version contains supplementary material available at https://doi.org/10.1038/s41598-026-39560-x.

Correspondence and requests for materials should be addressed to B.H. or H.W.

Reprints and permissions information is available at www.nature.com/reprints.

Publisher's note Springer Nature remains neutral with regard to jurisdictional claims in published maps and institutional affiliations.